Proceedings of NHTC'03
2003 ASME National Heat Transfer Conference
Las Vegas, NV, July 21-23, 2003

HT2003-47254

DYNAMIC BEHAVIOR OF CRYOGEN SPRAY COOLING: EFFECT OF SPRAY DISTANCE

G.-X. Wang

Department of Mechanical Engineering
The University of Akron
Akron, Ohio 44325-3903, USA

G. Aguilar[1,2] and J. S. Nelson[1,2]

[1]Department of Biomedical Engineering
University of California, Irvine, CA 92697
[2]Beckman Laser Institute
University of California, Irvine, CA 92612

ABSTRACT

Cryogen spray cooling (CSC) is used to minimize the risk of epidermal damage during laser dermatologic surgery. During CSC, skin surface is cooled by a short spurt of refrigerant R134a with boiling point of –26.2 °C. Since R134a is volatile in open atmospheric conditions, the atomized liquid droplets undergo continuous evaporation as they fly in air, leading to a lost momentum and mass. Therefore, the cooling effect of CSC depends strongly on the spray distance between the nozzle and the skin surface (L). The objective of this study was, therefore, to investigate the effect of L on the dynamic heat transfer of CSC. A skin model system made of poly methyl-methacrylate resin (Plexiglass®) is used to simulate CSC during laser dermatologic surgery. A fast-response temperature measurement sensor is built using thin (20 μm) aluminum foil and placed on top of the plexiglass with a 50 μm bead diameter thermocouple positioned in between. Variation of the surface temperature is then measured under various spray distances. The surface heat flux (q) as well as the heat transfer coefficient (h) between the surface and the cryogen is estimated by solving an inverse heat conduction problem with the measured temperature data as input. The effect of L on surface cooling in CSC is then investigated systematically. Both the estimated q and h show strong dynamic characteristics and are strong functions of the L. Two distinct spray-surface interaction mechanisms are identified within the spray distances studied.

For short L (< 30 mm), the spurt droplets impinge on the substrate violently, resulting in a fairly thin cryogen film deposited on the surface. Strong dynamics and high q result in this case, corresponding to a high h as well. Interestingly, h becomes strongly fluctuating and even larger after spurt termination for these cases. For long L (> 30 mm), q is lower and it steadily decreases after spurt termination. The dynamic variation of h in this case is similar to that of q.

These results should help in the selection of optimal CSC parameters, which are needed to produce high heat fluxes at the skin surface and thus obtain maximal epidermal protection during various dermatologic laser therapies.

Keywords: Laser dermatology, fast temperature sensor, inverse heat conduction.

INTRODUCTION

Cryogen spray cooling (CSC) is used in conjunction with various dermatologic laser surgeries [1,2,3,4]. Its purpose is to cool selectively the epidermis to prevent excessive epidermal heating after laser irradiation, while deeper targeted chromophores are thermally photocoagulated [5,6]. During CSC, the skin surface is sprayed with tetrafluoroethane (R-134a) for a short period of time (10-100 ms). R-134a in liquid state is released from a pressurized container through a valve–nozzle system and atomized into small droplets (3-20 μm)[7,8]. Since R-134a is volatile at atmospheric conditions, droplets evaporate while moving towards the skin surface at high speed (10-60 m/s) [7]. As a result, the low temperature (–26 to –60 °C) [7,8] of the impinging cryogen droplets can effectively cool the skin surface.

The main parameters that characterize spray cooling are the heat flux (q) through the skin surface and heat transfer coefficient, h. Studies to quantify q or h during CSC were carried out first by Anvari *et al*. [9], who measured the change in skin surface temperature using infrared thermometry. An average h value of 40 kW/m^{2}K was estimated using a cryogen layer temperature, $T_c = -7$ °C for spurt durations (Δt) ranging

from 5-80 ms with a nozzle-to-skin distance (L) of 20 mm. Torres *et al*. [10] later used an epoxy block with 30 μm thermocouples embedded at different depths ranging from 20 to 400 μm. Using this block to measure the internal temperatures during short cryogen spurts and an inverse heat conduction problem (IHCP) algorithm, Torres *et al.* [10] obtained a rather low value for h (~ 2.4 kW/m^{2}K) based on a constant $T_c \approx -44\ ^oC$. Recent studies using a refined IHCP algorithm [11], as well as other experimental techniques based on constant heat flux [12] or lumped capacitance [13,14] principles, showed that for similar CSC conditions, h varies between the two values previously reported [9,10].

It is clear, however, that to cool selectively the epidermis prior to laser irradiation, cryogen spurts should produce high heat fluxes at the skin surface and that two key parameters must be optimized: Δt and L. In clinical practice, it is possible to select different Δt, typically 10-100 ms. However, L is always fixed by the handpiece unique to each commercial device. Because cryogen droplets evaporate during flight, L should also be optimized to achieve higher heat fluxes.

A fast temperature sensor was recently introduced [15] with a response time on the order of a few milliseconds, which can measure rapid changes in the skin surface temperature during CSC. Systematic measurements of temperature changing under various spray conditions have been performed. Using the measured temperature data as input, an inverse heat conduction problem is solved to estimate the dynamic variation in q and h [16]. It was found [15] that there are two different surface cooling regimes, which depend on L. When L is greater than 25 mm, the spray is more finely atomized before reaching the surface and, therefore, a thicker cryogen layer forms on the skin surface. The presence of this layer prevents the skin surface from cooling beyond certain minimum and, therefore, impairs the heat extraction rate. In contrast, when L is less than 25 mm, larger and faster droplets impinge on the skin more forcefully, leading to a thinner cryogen layer that quickly evaporates. As a result, lower minimum temperatures are achieved and, consequently, the heat transfer is enhanced. This paper presents a detailed study of the effect of the spray distance on cooling effect during CSC.

EXPERIMENTAL SET-UP AND PROCEDURES

Temperature measurement sensor

The temperature sensor consists of a miniature type-K thermocouple (~ 50 μm bead diameter) placed underneath a thin (20 μm) layer of aluminum foil (15 mm × 10 mm) (Figure 1). The aluminum foil is positioned on top of a 12.5 mm square bar of poly methyl-methacrylate resin (Plexiglass®). Small strips of 50 μm thick cellulose tape (Scotch® tape) are placed between the aluminum foil and the Plexiglass® bar, forming a square box around the thermocouple bead and providing thermal insulation and mechanical support. Thermal paste is applied around the bead to ensure good thermal contact. The purpose of this sensor is to provide a skin-like thermal substrate, so that the overall heat extraction, Q, and surface heat extraction, q, are on the same order of magnitude as those expected for human skin. The small aluminum foil coupled with a miniature temperature sensor provides "real-time" surface temperature measurements. Published thermal properties of the materials used to build these sensors are shown in Table 1. Thermal properties of epidermal human skin [17] are also given for reference.

All thermocouple measurements are acquired at 4 kHz and converted to temperature data using an A/D converter board and dedicated software (InstruNet™, Omega Engineering, Stamford, CT). This acquisition rate is appropriate because the response time (τ) of the aluminum foil attached to the thermocouple sensor is less than 3 ms.

Cryogen delivery and nozzle

The cryogen utilized is R-134a, with boiling temperature $T_b \approx -26.2°C$ at atmospheric pressure. Cryogen is kept in a container at saturation pressure (660 kPa at 25°C), and delivered through a high-pressure hose to an electronically controlled fuel injector attached to a straight-tube nozzle. The nozzle is made of stainless steel with an inner diameter (d_N) and length (l_N) of 0.7 mm and 63.6 mm, respectively. The nozzle is soldered to a custom-made copper coupling, which in turn fits tightly around the fuel injector. The nozzle diameter is similar to that of commercial devices.

MATHEMATICAL MODEL AND INVERSE HEAT TRANSFER ALGORITHM

CSC dynamics can be simplified to a one-dimensional heat conduction problem if a uniform heat transfer over the sprayed surface (Figure 1) is assumed. An IHCP algorithm is solved using the measured surface temperature as input. Many algorithms have been developed to solve such an inverse problem [18,19] and the Sequential Function Specification Method (SFSM) of Beck *et al.* [19] is employed here. SFSM estimates q as a piecewise constant function of time, sequentially solving for q at each time step. Tunnell *et al.* [11] provided a detailed discussion of this algorithm as applied to CSC.

Using the layered structure and the coordinate system given in Figure 1, the SFSM solves a one-dimensional heat conduction problem given by Equation (1):

$$\rho_j c_j \frac{\partial T_j}{\partial t} = k_j \frac{\partial^2 T_j}{\partial y^2} \qquad (1)$$

where ρ is density, c is specific heat, k is thermal conductivity and the subscript j is replaced by *Al*, *ST*, or *PG* when Eq. 1 is applied to the aluminum foil, scotch tape, and Plexiglass® layers, respectively. The Plexiglass® can be treated as a semi-infinite thick body and, thus, only one boundary condition at the aluminum foil surface is needed:

$$-k_{Al}\left.\frac{\partial T_{Al}}{\partial y}\right|_{y=b} = q(t) \qquad (2)$$

where b is the aluminum foil thickness and $q(t)$ is the surface heat flux that must be estimated.

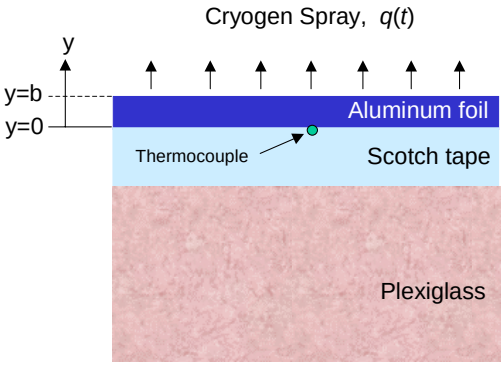

Figure 1. Schematic of the thin Al-foil experimental sensor.

Properties	Al foil	Scotch Tape ®	Plexiglass ®	Epidermis
thick [mm]	0.020	0.050	19	--
k [W/(m K)]	205	0.19-0.25	0.19-0.24	0.21
ρ [kg/m^3]	2,710	1,160-1,400	1,150-1,190	1,200
c [J/(kg K)]	896	1,400	1,300-1,500	3,600
α_{avg} [m^2/s]	844×10^{-7}	1.22×10^{-7}	1.31×10^{-7}	0.486×10^{-7}

Table 1. Thermal properties and thicknesses of layers used in the temperature measurement sensor. Human epidermal skin properties are provided for reference.

SFSM assumes a functional form of the surface heat flux variation over any given discrete time period. The simplest function form is that $q(t)$ is a constant, which is used here. For an assumed constant heat flux (q_M^*) over time t_M to t_{M+1}, the governing equations 1 and 2 are solved for times t_M, t_{M+1}, … , t_{M+r-1}, giving temperatures T_M^*, T_{M+1}^*, …, T_{M+r-1}^* at corresponding time points at y = 0, where the temperature was measured during the experiment. One important feature of SFSM is that it uses the temperature information of future time steps, with r being the number of future time steps. More stable and physically sound results are obtained using multiple future steps, *i.e.*, $r \geq 2$. In that case, the actual surface heat flux, q_M, can be calculated based on the assumed heat flux, q_M^* [11,19]:

$$q_M = q_M^* + \frac{\sum_{i=1}^{r}(Y_{M+i-1} - T_{M+i-1}^*)Z_{i-1}}{\sum_{i=1}^{r}\left(Z_{i-1}\right)^2} \qquad (3)$$

where Z_i is the sensitivity coefficient, defined as:

$$Z_i = \frac{\partial T_i}{\partial q_M} \qquad \text{at } y = 0, \qquad (4)$$

and Y_i is the measured temperature at time t_i. The sensitivity coefficient can be obtained by solving Eq. (1) with T_j replaced by Z_i but with a boundary condition:

$$-k_{Al}\left.\frac{\partial Z_i}{\partial y}\right|_{y=b} = 1 \qquad (5)$$

under the same geometrical conditions.

DATA SMOOTHING AND ANALYSIS

Raw data are affected by fluctuations, which may include random and AC noise. Thus, independent of the specific mathematical technique used in the IHCP, smoothing of the data is required for the numerical computation of first - or higher-order derivatives. For the data presented herein, a digital filter of least squares fitting with orthogonal Gram polynomial of third degree [18] is used for first-order derivatives only:

$$Y_M = Y(t_M) = \frac{1}{429}\left(\begin{array}{l} -36Y_{i-5} + 9Y_{i-4} + 44Y_{i-3} + 69Y_{i-2} + 84Y_{i-1} \\ +89Y_i + 84Y_{i+2} + 69Y_{i+2} + 44Y_{i+3} + 9Y_{i+4} - 36Y_{i+5} \end{array}\right) . \qquad (6)$$

Calculations indicate that such a digital filter is very effective in removing random noise.

RESULTS AND DISCUSSION

Figure 2a shows the time variation of the surface temperature produced by 60 ms spurts delivered at spray distances (L) varying between 15–40 mm. As seen, the surface temperature drops rapidly from room to below the cryogen boiling temperature, T_b for all L, reaching a minimum temperature (T_{min}) of ~ –40 °C for spurts at $L \leq 25$ mm. It is also clear that for $L \leq 25$ mm, the surface remains below T_b for a relatively short time, and it is quickly warmed up above T_b before 300 ms after spurt initiation. However, for $L > 25$ mm, the surface temperature remains close to T_b for a fairly long time, reaching 1000 ms for L = 40 mm. The time the surface temperature is at or near T_b has a physical meaning, as it can be related to the time cryogen liquid film resides on the sprayed surface before it evaporates completely, hereafter referred to as the residence time t_r.

Figure 2b shows the results for spurts delivered at L between 40–80 mm. In contrast with T_{min} = –40°C for $L \leq 25$ mm seen in Fig. 2a, a T_{min} of –32°C is reached for all spurts shown in Fig. 2b. By further increasing L, however, t_r becomes shorter again. This indicates that L = 40 mm is the distance at which a maximum deposition of cryogen droplets is reached, forming the thickest cryogen layer and, thus, the longest t_r.

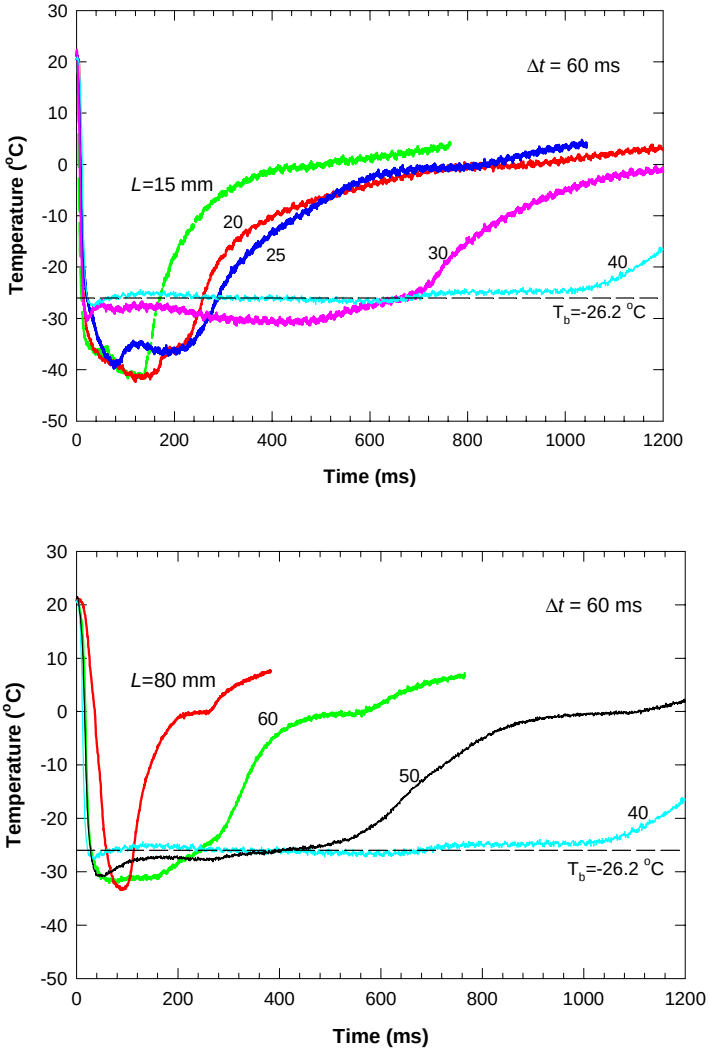

Figure 2. Measured temperature variations as a function of time for various spray distances L: (a) 15, 20, 25,30 and 40, (b) 40, 50, 60, and 80. Spurt duration: Δt = 60 ms.

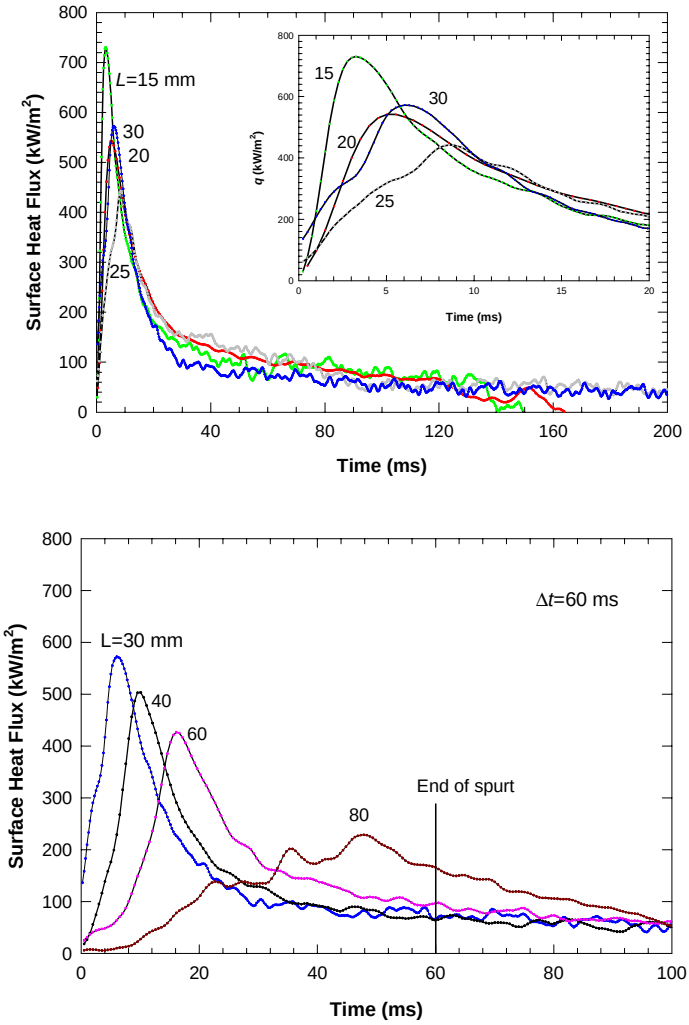

Figure 3. Estimated surface heat flux as a function of time for various spray distances L: (a) 15, 20, 25, and 30, (b) 30, 40, 60, and 80. Spurt duration: Δt = 60 ms.

Also shown in the insert of Figure 3a is the continuous decrease in the maximum heat flux, q_{max} as L increases from 15 to 25 mm. Increasing L from 25 to 30 mm, however, leads to an enhanced q_{max}, consistent with the sharp change in the surface temperature dynamics observed in Fig. 2a between these two values of L. Further increasing L beyond 30 mm results in a continuous decrease of q_{max} and a broadening of the peak region of high q, as shown in Fig. 3b.

Using the temperature data shown above, the surface heat flux (q) was estimated as a function of time by solving the IHCP algorithm. Figures 3a and 3b show the time variation of q for spurts at L =15-30 mm and L = 30-80 mm, respectively. In all cases, the variation in q shows a strong dynamic behavior and it is evident that high q is achieved only during the first 20 ms after spurt initiation.

It is interesting to note that despite the differences in the dynamic behavior of the surface temperatures for all the L tested, a unique and fairly steady q of ~ 100 kW/m^2 is reached before spurt termination (~ 25-30 ms), which corresponds roughly to the time it takes the surface to reach a temperature below T_b, after which the substrate cooling is primarily dominated by heat conduction through the liquid cryogen layer deposited on the substrate's surface during the spurt, and by the cryogen evaporation to the environment at the cryogen layer/air interface. Indirect proof of the presence of this layer is also evident from the data shown in Figs. 2a,b, where the surface temperature oscillates around T_b for a long time until the liquid cryogen has completely evaporated and the surface temperature increases thereafter.

The variation of q_{max} with L seen in Figs. 3a,b is non-linear and this can be illustrated in Figure 4, where q_{max} is plotted as a function of L. In this form, it becomes evident that there exist two different surface cooling regimes with the transition taking place at L = 25–30 mm. Fig.4 also shows the results for somewhat longer spurts (Δt = 100 ms), where q_{max} was measured at the same L. Both curves appear to collapse into one, suggesting that the existence of these two regimes is independent of Δt.

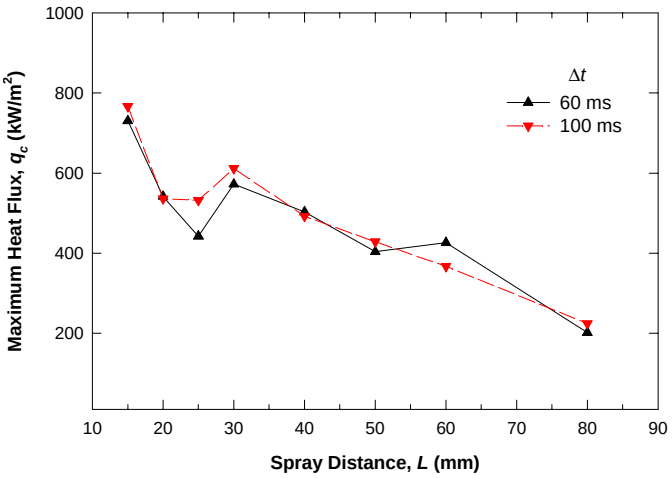

Figure 4. Maximum heat flux achieved for as a function of spray distance L.

Figure 5 shows the minimum surface temperature, T_{min} that was measured as a function of L for each of the 60 ms spurts used for this study (T_{min} was obtained from the temperature data shown in Figures 2a,b). The same transition region between the two cooling regimes and the non-linear variation of surface temperature and q pointed out in Figs. 2a,b and 4, can be observed again in this case. Figure 5 also shows previous results [16] of steady state average cryogen spray temperature measurements, T_s that were obtained by inserting miniature thermocouples at different locations into the spray cone, for spurts produced by the same nozzle used herein. In contrast with T_{min}, it is seen that T_s drops continuously and almost linearly with L. It is thus clear that whereas spray temperature is solely dictated by the evaporation dynamics of cryogen droplets in-flight when unobstructed by a solid surface [8], there are more complex heat transfer mechanisms taking place at the cryogen spray/surface interface during CSC.

Using the measured surface temperature and T_s, the computed q can be converted into the heat transfer coefficient h, which is also a function of time. Figures 6a and 6b show the dynamic variation of h as function of time for L = 15-30 mm and L = 30-80 mm, respectively. As one could expect, the variation of h is also rather different for the two identified cooling regimes.

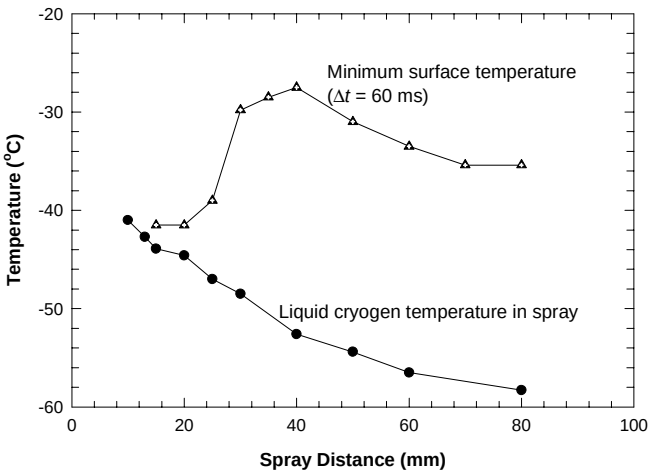

Figure 5. Minimum surface temperature reached during 60 ms spurts (triangles) and the corresponding spray cryogen temperature (circles) as a function of L.

At the shortest spray distance, L = 15 mm, the variation of h shows a strong dynamic change, even after spurt termination. Note that h increases quickly to a maximum value h_{max} of ~ 25 kW/m^{2}K within 14 ms, and then drops fairly fast to below 10 kW/m^{2}K upon spurt termination (60 ms). This variation follows closely that of q shown in Figure 3a. A distinct feature, in the dynamics of h at this spray distance is, however, the strong dynamic fluctuation of h near the end of the spurt and afterwards. This strong fluctuation seems to start at about 30 ms and become stronger after spurt termination, even reaching a higher magnitude of h than that seen during the spurt. Similar variations in h can also be observed for L = 20 and 25 mm, except that the maximum in h during the spurt is not as obvious as for L = 15 mm. As discussed above, a transition region takes place between 25-30 mm, and just as q_{max} becomes higher for L = 30 mm than for L = 25 mm, the same happens with h_{max}. Also, the strong fluctuations and higher h values seen for $L \leq 25$ mm after spurt termination disappear for $L \geq 30$ mm and h_{max} continues to decrease gradually as L increases, as shown in Figure 6b.

Figure 7 shows the variation of h with time, each variable normalized by h_{max} and t_{max}, respectively, where t_{max} is the time it takes for h to reach h_{max}. In this representation, there is clearly a closer similarity among all curves for L = 30–60 mm, except for L = 80 mm, where there appears to be stronger fluctuation and the curve drops faster without the long decay that the others show.

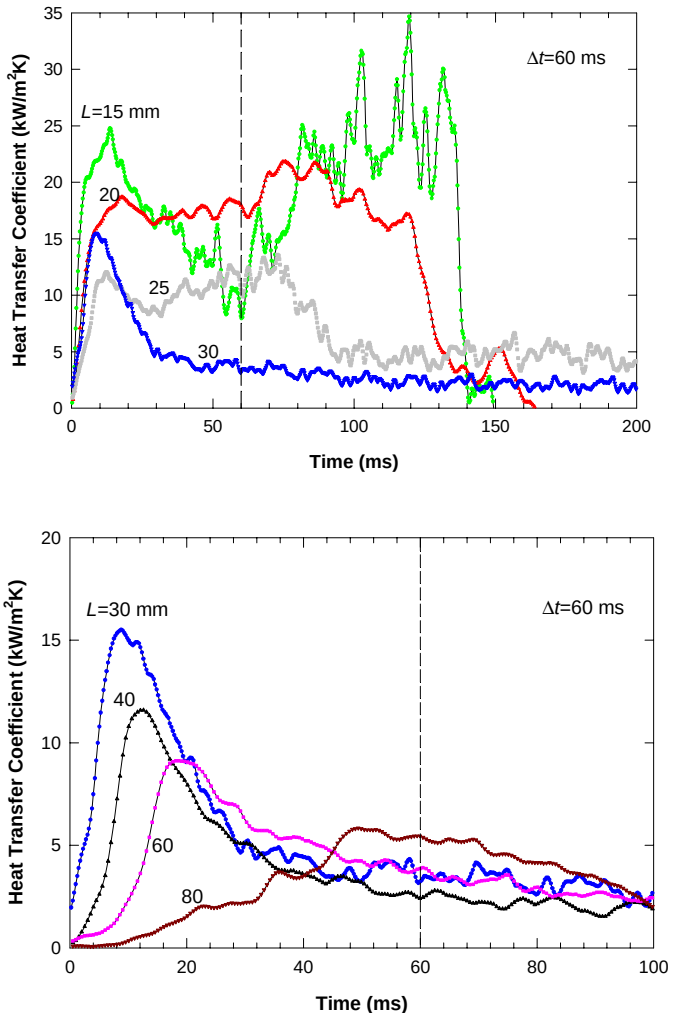

Figure 6. Estimated heat transfer coefficients h, as a function of time for various spray distances L: (a) 15, 20, 25, and 30, (b) 30, 40, 60, and 80. Spurt duration: Δt = 60 ms.

Besides the dynamic variation in q and h, the total heat removal per unit area Q is an important consideration for various applications, such as those related to dermatologic laser therapy. Q can be easily determined by integrating q over time. Figure 8 shows how Q varies as a function of L for some selected values of L. It is seen that the variations in Q also reflect different heat transfer characteristics at different L, as discussed above. For L = 20 and 80 mm Q reaches a maximum and it even decreases within the 250 ms window shown in Fig. 8. The reduction in Q indicates that the liquid cryogen deposited has evaporated and, thus, warm air transfers heat back to the surface. Interestingly, although qualitatively the same behavior for these two extreme cases (20 and 80 mm), the reason for the presence of a thin cryogen layer is different. For the 20 mm case, the cryogen layer is thin due to a very forceful impact of the cryogen spray on the surface and the radial spreading of the liquid cryogen. For the case of 80 mm, the cryogen layer is thin due to the lesser amount of cryogen droplets reaching the surface because of in-flight evaporation. For the intermediate L values (30 and 50 mm), the maximum Q is not even seen within the 250 ms shown in this figure, suggesting that the cryogen layer is relatively thick and, therefore, the residence time (t_r) is longer, which is why heat is still being extracted from the surface even at 250 ms.

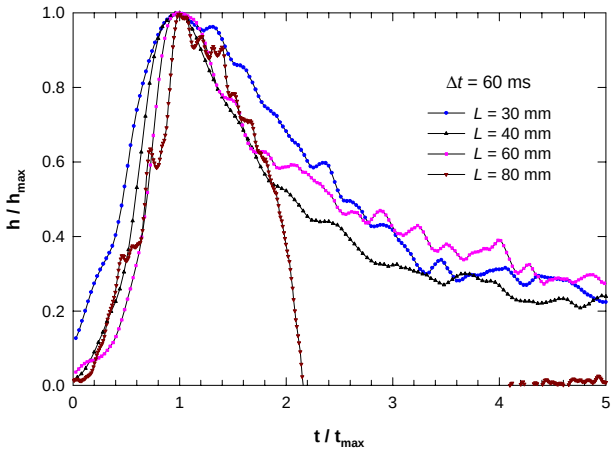

Figure 7. Normalized h, ($h/h_{\max}$) as a function of normalized time ($t/t_{\max}$), where t_{max} is the time it takes h_{max} to be reached.

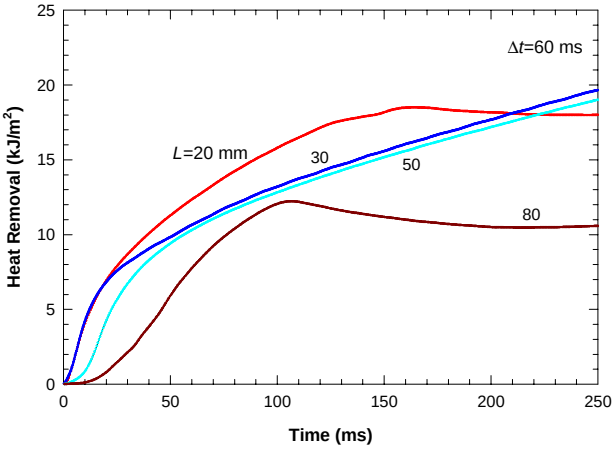

Figure 8. Total heat removal per unit area Q, as a function of time for various spray distances L: 20, 30, 50, and 80. Spurt duration: Δt = 60 ms.

CONCLUSIONS

Experiments have been performed to investigate the heat transfer dynamics during CSC using a fast-response temperature sensor. An IHCP algorithm is used to estimate the surface heat flux (q) and the heat transfer coefficient (h) as functions of time. The effect of spray distance (L) on dynamic heat transfer characteristics of CSC is systematically investigated and presented in this paper.

In all cases, q reveals a marked dynamic variation during CSC with a maximum heat flux (q_{max}) occurring during the

early stages of the spurt, followed by a quick decrease. *L* has a strong effect on CSC with very different surface dynamics resulting from short and long *L*. For short *L* (< 30 mm), the spurt is more jet-like with droplets impinging the substrate violently, resulting in a fairly thin cryogen film deposited on the surface. Strong dynamics and high *q* result in this case, corresponding to a high *h* as well. Interestingly, *h* becomes strongly fluctuating and even larger after spurt termination for *L* < 30 mm. For long *L* (> 30 mm), *q* is lower and it steadily decreases after spurt termination. The dynamic variation of *h* in this case is similar to that of *q*.

In summary, *L* = 15-20 mm appears to produce near maximum *q*, *h*, and *Q* and, thus, for this particular nozzle, this range of *L* would seem to be the best suited for optimal laser therapy of vascular lesions. However, one should be aware that the shorter the *L* is, the more confined the sprayed area would be, in addition to the more painful spray deposition could result for the patient.

ACKNOWLEDGMENTS

This work was supported by the National Institutes of Health (GM 62177 to JSN and HD42057 to GA). Institutional support from the Beckman Laser Institute Endowment is also acknowledged. Laboratory assistance and data analysis provided by Emil Karapetian, Odette Ma and Misha Heller are greatly appreciated.

REFERENCES

1 J.S. Nelson, T.E. Milner, B. Anvari, B.S. Tanenbaum, S. Kimel, L. O. Svaasand, and S. L. Jacques, "Dynamic epidermal cooling during pulsed laser treatment of port-wine stain", *Arch. Dermatol.*, vol. 131, 695-700, 1995.

2 H.A. Waldorf, T.S. Alster, K. McMillan, A.N. Kauvar, R.G. Geronemus, and J. S. Nelson, "Effect of dynamic cooling on 585-nm pulsed dye laser treatment of port-wine stain birthmarks," *Dermatol. Surg.*, vol. 23, 657-662, 1997.

3 C.J. Chang, B. Anvari, and J.S. Nelson, "Cryogen spray cooling for spatially selective photocoagulation of hemangiomas: a new methodology with preliminary clinical reports," *Plast. Reconstr. Surg.*, vol. 102, 459-463, 1998.

4 K.M. Kelly, J.S. Nelson, G.P. Lask, R.G. Geronemus, and L.J. Bernstein, "Cryogen spray cooling in combination with non-ablative laser treatment of facial rhytides," *Arch. Dermatol.*, vol. 135, 691-694, 1999.

5 J.S. Nelson, B. Majaron and K.M. Kelly, "Active skin cooling in conjunction with laser dermatologic surgery: Methodology and clinical results," *Sem. Cut. Med. Surg.*, vol. 19, 253-266, 2000.

6 W. Verkruysse, B. Majaron, B.S. Tanenbaum, and J.S. Nelson, "Optimal cryogen spray cooling parameters for pulsed laser treatment of port wine stains," *Lasers Surg Med*, vol. 27, pp. 165-170, 2000.

7 G. Aguilar, B. Majaron, W. Verkruysse, J.S. Nelson, and E.J. Lavernia, "Characterization of cryogenic spray nozzles with application to skin cooling," In Proceedings: *International Mechanical Engineering Congress and Exposition* (IMECE), Orlando FL, FED-v. 253, pp. 189-197, 2000.

8 G. Aguilar, B. Majaron, W. Verkruysse, Y. Zhou, J.S. Nelson, and E.J. Lavernia, "Theoretical and experimental analysis of droplet diameter, temperature, and evaporation rate evolution in cryogenic sprays," *Int. J. Heat Mass Transfer*, vol. 44, 3201-3211, 2001.

9 B. Anvari, T.E. Milner, B.S. Tanenbaum, and J.S. Nelson, "A comparative study of human skin thermal response to sapphire contact and cryogen spray cooling," *IEEE Trans. Biomed. Eng.*, vol. 45, pp. 934-941, 1998.

10 J.H. Torres, J.W. Tunnell, B. Pikkula, and B. Anvari, "An analysis of heat removal during cryogen spray cooling and effects of simultaneous airflow application," *Lasers Surg. Med.*, vol. 28, 477- 486, 2001.

11 J.W. Tunnell, J.H Torres, and B. Anvari, "Methodology for estimation of time-dependent surface heat flux due to cryogen spray cooling," *Annals Biomed. Eng.*, vol. 30, 19-33, 2002.

12 G. Aguilar, W. Verkruysse, B. Majaron, L.O. Svaasand, E.J. Lavernia, and J.S. Nelson, "Measurement of heat flux and heat transfer coefficient during continuous cryogen spray cooling for laser dermatologic surgery," *IEEE J Special Topic Quantum Electr.*, vol. 7, 1013-1021, 2001.

13 L.O. Svaasand, L.L. Randeberg, G. Aguilar, B. Majaron, S. Kimel, E.J. Lavernia, and J.S. Nelson, "Cooling efficiency of cryogen spray during laser therapy of skin" *Lasers Surg Med*, vol. 32, pp.137-142, 2003.

14 G. Aguilar, B. Majaron, K. Pope, L.O. Svaasand, E.J. Lavernia, and J.S. Nelson, "Influence of nozzle-to-skin distance in cryogen spray cooling for dermatologic laser surgery", *Lasers Surg Med*, vol. 28, pp.113-120, 2001.

15 G.. Aguilar, G.-X. Wang, and J.S. Nelson, "Dynamic cooling behavior during cryogen spray cooling: effects of spurt duration and spray distance," *Lasers Surg Med*, vol. 32, pp.152-159, 2003.

16 G.. Aguilar, W. Verkruysse, B. Majaron, L.O. Svaasand, E.J. Lavernia, and J.S. Nelson, "Measurement of heat flux and heat transfer coefficient during continuous cryogen spray cooling for laser dermatologic surgery", *IEEE J Special Topic Quantum Electr*, vol. 7, pp. 1013-1021, 2001.

17 F.A. Duck, "Thermal properties of tissue", In: Physical properties of tissue. London: Academic Press, 1990.

18 J. Taler, "Theory of transient experimental techniques for surface heat transfer," *Int. J. Heat mass transfer*, vol. 39, pp. 3733-3748, 1996.

19 J.V. Beck, B. Blackwell, and C.R. St. Clair CR, *Inverse heat conduction: Ill-posed problems*, New York, NY, Wiley, 1985.